nature photonics

Article

https://doi.org/10.1038/s41566-023-01209-w

Photon-statistics force in ultrafast electron dynamics

Received: 21 September 2022

Accepted: 6 April 2023

Published online: 5 June 2023

Check for updates

Matan Even Tzur[1,3] ✉, Michael Birk[1,2,3], Alexey Gorlach[2], Michael Krüger[1], Ido Kaminer[2] & Oren Cohen[1] ✉

In strong-field physics and attosecond science, intense light induces ultrafast electron dynamics. Such ultrafast dynamics of electrons in matter is at the core of phenomena such as high-harmonic generation, where these dynamics lead to the emission of extreme-ultraviolet bursts with attosecond duration. So far, all ultrafast dynamics of matter were understood to purely originate from the classical vector potential of the driving light, disregarding the influence of the quantum nature of light. Here we show theoretically that the dynamics of matter driven by bright (intense) light significantly depend on the quantum state of the driving light through its quantum noise, which induces an effective photon-statistics force. To provide a unified framework for the analysis and control over such a force, we extend the strong-field approximation theory to account for non-classical driving light. Our quantum strong-field approximation theory shows that in high-harmonic generation, experimentally feasible squeezing of the driving light can shift and shape electronic trajectories and attosecond pulses at the scale of hundreds of attoseconds. Our work presents a new degree of freedom for attosecond spectroscopy, by relying on non-classical electromagnetic fields, and more generally, introduces a direct connection between attosecond science and quantum optics.

Ultrafast electron dynamics driven by intense light is central to all phenomena in strong-field physics and attosecond science[1]. Examples include attosecond interferometry[2,3], attosecond bandgap dynamics[4], ultrafast chiral detection[5,6] and more[7,8]; the prime example being high-harmonic generation (HHG) (refs. 9–13). HHG occurs when an intense light field drives matter (gases[9–11], liquids[14], solids[15] or plasma[16]) to emit a train of attosecond pulses[17], which spectrally consists of high-order harmonics of the driving field. HHG in the gas phase is intuitively understood in terms of the three-step model[11–13]: an initially bound electron undergoes laser-induced tunnel ionization, then accelerates in the continuum by the oscillating laser field and finally recombines with its parent ion, releasing its kinetic and potential energy as a high-energy photon.

Soon after its inception, the classical three-step model[12] was generalized by Lewenstein et al. to a quantum mechanical setting[13], where matter is quantum and light is classical. Lewenstein's model, also known as the strong-field approximation (SFA) theory, allows for both quantitative analysis and intuitive understanding of attosecond pulse generation during HHG in terms of ultrafast electron dynamics. In particular, the duration and chirp of attosecond pulses are directly correlated with electronic recombination times, and indirectly correlated with ionization times and canonical momenta of the electronic trajectories. Indeed, the SFA theory plays a critical role in the development of attosecond science[18,19].

Nevertheless, so far, the SFA theory remained semi-classical—it did not account for the quantum nature of the driving light[20]. The

[1]Solid State Institute and Physics Department, Technion—Israel Institute of Technology, Haifa, Israel. [2]Solid State Institute and Department of Electrical and Computer Engineering, Technion—Israel Institute of Technology, Haifa, Israel. [3]These authors contributed equally: Matan Even Tzur, Michael Birk. ✉e-mail: Matanev@campus.technion.ac.il; Oren@technion.ac.il

reason for this was twofold. First, since the driving pulse contains a macroscopic number of photons, its quantum nature was expected to be inconsequential, that is, only the classical vector potential of the light field plays any role in the induced dynamics. Second, all the experiments in strong-field physics and attosecond science used classical driving fields (that is, Glauber coherent states[21]), as it was thought to be the only state of light accessible with high intensities and ultrashort pulse durations. Importantly, this situation is now rapidly changing, because ultrashort pulses of intense non-classical light are becoming well-established drivers of nonlinear optics[22–24], starting to approach the regime of strong-field physics[22,25–28]. This rapid advance motivates us to revisit the established SFA theory and consider the effect of the quantum photon statistics of the driving light on the ultrafast dynamics of electrons. Insight into the dynamics of electrons in bright quantum fields is especially timely considering the recent developments in quantum optical strong-field physics. Many years after the early quantum electrodynamical investigations of HHG[29,30], this field is reignited by recent photon-counting experiments[31], and it continues to develop as a platform for quantum information processing, for example, through the generation of photonic cat states[32]. Additionally, quantum optical strong-field physics plays a fundamental role in the explorations of light–matter entanglement[33–36] and other examples[37].

Here we present the framework of quantum strong-field approximation (qSFA), extending Lewenstein's SFA theory to account for non-classical states of intense light that drive atoms or other emitting systems[38]. The framework of qSFA reveals a new effect: ultrafast dynamics of strongly light-driven matter significantly depends on the quantum state of the driving light, and particularly on its photon statistics. We study this effect in detail for the example of squeezed light and show that experimentally feasible squeezing of the driver's photonic state modifies HHG ionization and recombination times by hundreds of attoseconds. Moreover, this modulation of electronic trajectories by squeezing leaves a pronounced mark on the temporal profile of the emitted attosecond pulses and on the HHG spectrum. We further show how to explain these phenomena in terms of short and long trajectories. Finally, we interpret our results in terms of an effective photon-statistics force, which is applied by the squeezed pump on the electronic system. In general, the qSFA framework opens the way for the fusion of quantum optics with attosecond science, and for time-resolved insights into the role of the quantum nature of light in the interplay between three of the most fundamental processes in physics—ionization, recombination and acceleration of charged particles by photons.

Results

Quantum optical SFA

The main result of the semi-classical SFA theory is an analytical formula for the dipole-moment expectation value of an atom in bright (and classical) laser light. This result played a central role in the development of attosecond science over the years, as it connects HHG emission with the underlying electronic dynamics. In this section, we generalize this result and derive an analytical formula for the dipole-moment expectation value for an electron driven by an arbitrary quantum state of light. To do so, we decompose the quantum state of the driving light to semi-classical Glauber coherent states, where each coherent state is denoted by $|\alpha\rangle$. We find that within the SFA, the dipole-moment expectation value $z(t)$ of an electron driven by such a superposition state is given by $z(t) = \int \mathrm{d}^2\alpha P(\alpha) z_\alpha(t)$, where $P(\alpha)$ is a distribution of coherent states specifying the quantum state of the driver and $z_\alpha(t)$ are semi-classical dipole moments corresponding to an electron driven by coherent state $|\alpha\rangle$.

We begin by considering an atomic system that interacts with light of an arbitrary quantum state that can be approximated as a single mode during the interaction process. The ionization potential of this atomic system is denoted by I_p. The density matrix of the driving light is specified by the positive P representation[39] $P(\alpha,\beta)$:

$$\hat{\rho}_\mathrm{drive} = \int d^2\alpha\, d^2\beta\, P(\alpha,\beta) \frac{|\alpha\rangle\langle\beta^*|}{\langle\beta^*|\alpha\rangle}. \tag{1}$$

Here $|\alpha\rangle = |\alpha_x + \mathrm{i}\alpha_y\rangle$ is a coherent state of light, where α_x and α_y are real-valued parameters that correspond to a classical electromagnetic wave whose vector potential is given by[40]

$$\begin{aligned}\mathbf{A}_\alpha(t) &= \frac{\epsilon^{(1)}}{\omega}\left(\alpha \mathrm{e}^{-\mathrm{i}\omega t} + \alpha^* \mathrm{e}^{\mathrm{i}\omega t}\right)\hat{z} \\ &= \frac{2\epsilon^{(1)}}{\omega}\left[\alpha_x \cos(\omega t) + \alpha_y \sin(\omega t)\right]\hat{z}.\end{aligned} \tag{2}$$

Here ω is the angular frequency of the field, $\epsilon^{(1)} = \sqrt{\hbar\omega/2\epsilon_0 V}$ is the so-called single-photon-amplitude[40] and V is the volume of quantization, which will be eventually eliminated through the limit $V\to\infty$. The polarization is linear along $\hat{z}$. The corresponding electric field is given by $E_\alpha(t) = -\left(\partial\mathbf{A}_\alpha/\partial t\right)\cdot\hat{z} = 2\epsilon^{(1)}\left[-\alpha_x \sin(\omega t) + \alpha_y \cos(\omega t)\right]\hat{z}$.

The density matrix of an electron driven by $\hat{\rho}_\mathrm{drive}$ is (Supplementary Section I)

$$\hat{\rho}_\mathrm{e} = \int d^2\alpha d^2\beta P(\alpha,\beta^*)\, |\phi_\alpha(t)\rangle\langle\phi_\beta(t)|, \tag{3}$$

where $|\phi_{\alpha,\beta}\rangle$ are solutions to the semi-classical time-dependent Schrödinger equation (TDSE):

$$\mathrm{i}\hbar\frac{\partial|\phi_{\alpha,\beta}(t)\rangle}{\partial t} = \left[-\frac{1}{2m}\nabla^2 + U(z) - ez\cdot E_{\alpha,\beta}(t)\right]|\phi_\alpha(t)\rangle. \tag{4}$$

in which $U(z)$ is the atomic potential. Most generally, the dipole-moment expectation value is given by

$$z(t) = \mathrm{Tr}\left[\rho_\mathrm{e}(t)\, z\right] = \int d^2\alpha d^2\beta P(\alpha,\beta^*)\langle\phi_\beta(t)|\, z\, |\phi_\alpha(t)\rangle. \tag{5}$$

Neglecting ground state depletion, keeping only bound-continuum transitions[13] and utilizing the property $P(\alpha,\beta) = P(\beta,\alpha^*)$ of the positive P representation, we may write the dipole-moment expectation value as (Supplementary Section II)

$$z(t) = \int d^2\alpha P(\alpha)\, z_\alpha(t), \tag{6}$$

in which $z_\alpha(t)$ is the dipole-moment expectation value for a coherent-state drive $|\alpha\rangle$ and $P(\alpha) = \int \mathrm{d}^2\beta P(\alpha,\beta^*)$. This $P(\alpha)$ value is not to be confused with the Glauber–Sudarshan P representation (Supplementary Section II). Equation (6) quantifies the dipole for a driving field with arbitrary photon statistics. This dipole is later used to derive the HHG spectrum and pulse shape and is therefore a central result of this work. Finally, we take the limit where the single-photon amplitude $\epsilon^{(1)}$ approaches zero (that is, infinite quantization volume V), as the intensity (photon density) of the driving photonic state is kept constant. In this limit, $P(\alpha)$ of a coherent state reduces to a Dirac delta function (Supplementary Section III).

In the next section, we focus on squeezed coherent (SC) light, for which bunching is dominated by the coherent-state component of the field, and ground-state depletion enhancement is insignificant[41] (Supplementary Section VII), and hence, the transition between equations (5) and (6) is valid. This transition is not justified when multiphoton ionization is enhanced by photon bunching, for example, in the case of stochastic[42,43] and bright squeezed vacuum[44] pumps.

https://doi.org/10.1038/s41566-023-01209-w

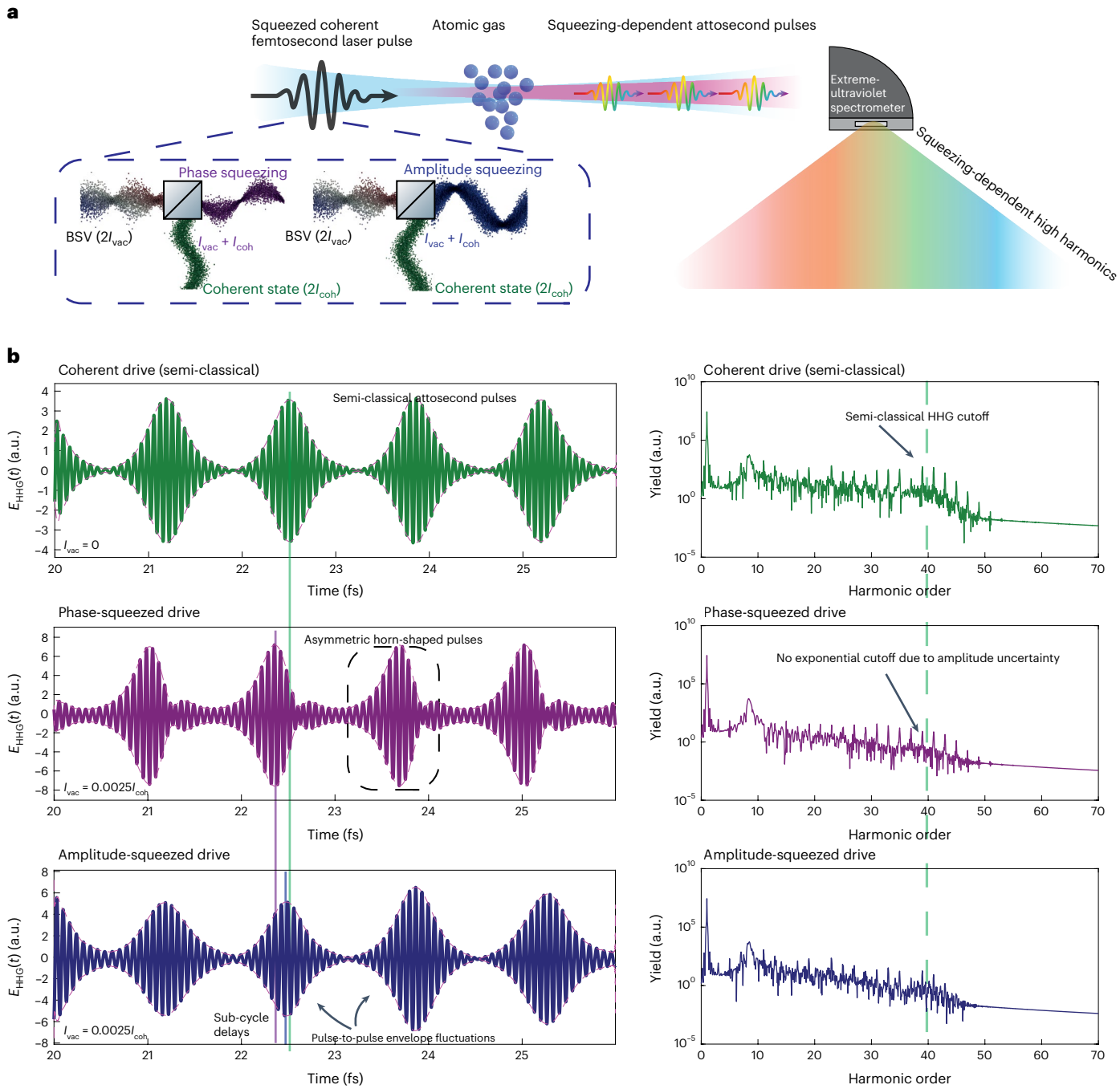

Fig. 1 | Squeezing-dependent generation of attosecond pulses and high-order harmonics. a, Schematic illustration of HHG driven by squeezed coherent light[52]. **b**, Exemplary attosecond pulses and HHG spectra driven by the following: classical light (top; green), that is, coherent state $|\alpha, 0\rangle$; phase-squeezed coherent state $|\alpha, r\rangle$ (centre; purple); and amplitude-squeezed coherent state $|\alpha, -r\rangle$ (bottom; blue). The plots in all the panels of both figures are based on equation (7a), choosing a squeezing parameter r that satisfies $\sinh^2(r) = 0.0025|\alpha|^2$, where α is normalized to correspond to an average intensity of 2×10^{14} W cm^{-2}. Explicitly, the parameters we choose for phase-squeezed driving light are $E_{\gamma_y} = 0.0756$ a.u., $E_{\gamma_x} = 0$ and $E_{vac} = \sqrt{0.0025}E_{\gamma_y}$, and those for amplitude-squeezed driving light are $E_{\gamma_y} = 0$, $E_{\gamma_x} = 0.0756$ a.u. and $E_{vac} = \sqrt{0.0025}E_{\gamma_x}$.

HHG driven by squeezed coherent light

The previous section formulates how the quantum nature of light alters the dynamics in light–matter interactions. Under the qSFA, the main effect on the dynamics is due to photon statistics. Qualitatively, this means that one could have two driving fields carrying the same classical vector potential but differing in photon statistics resulting in different material dynamics. In this section, we further investigate this effect, focusing on SC driving light fields. An SC field is denoted by $|\gamma = \gamma_x + i\gamma_y, r\rangle$, where r denotes the degree of squeezing and γ represents the coherent-state part that has vector potential $\mathbf{A}_\gamma(t)$ (equation (2)). The photon number of the SC field is $N_{|\gamma,r\rangle} = |\gamma|^2 + \sinh^2(r)$. Such a field can be generated by combining a strong coherent-state beam with a comparatively weak (~1%) squeezed vacuum beam[45]. The squeezing phase may be tuned by adjusting the phases between the coherent

https://doi.org/10.1038/s41566-023-01209-w

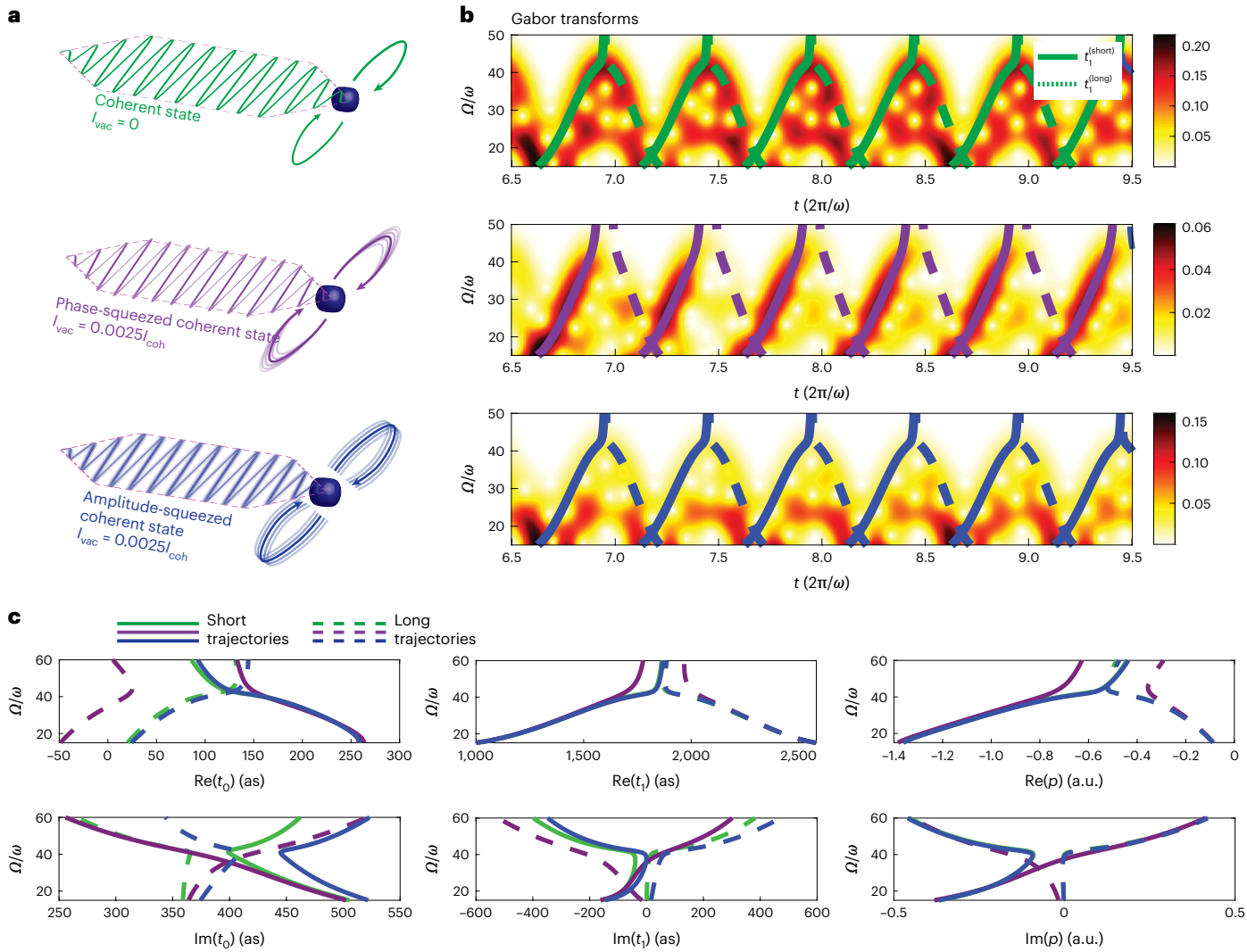

Fig. 2 | Three-step model in a quantized field and the resulting electronic trajectories. a, Illustrative distributions of semi-classical electronic dynamics from a coherent state driver (green), phase-squeezed coherent state (purple) and amplitude-squeezed coherent state (blue). Integration over these distributions results in the electronic dynamics in the quantum field. **b**, Time–frequency analysis (Gabor transform) of the dipole acceleration of an atom driven by the light states discussed above, overlaid with the real parts of the recombination times of short and long trajectories. **c**, Solutions of stationary parameters [p, t_1, t_0] for the cases of coherent state (green), phase squeezing (purple) and amplitude squeezing (blue). The parameters for coherent and squeezing conditions in Fig. 1 are used here.

and squeezed vacuum arms (Fig. 1). The squeezing parameter r is set (without loss of generality) to be real and positive henceforth, that is, the x quadrature is squeezed.

Inserting the $P(\alpha)$ distribution associated with $|\gamma, r\rangle$ into equation (6) and changing the integration variables to electric-field quadratures $E_{\alpha_x} = 2\epsilon^{(1)}\alpha_x$ and $E_{\alpha_y} = 2\epsilon^{(1)}\alpha_y$ leads to an expression for the dipole moment induced by the interaction of an atom with such an SC state (Supplementary Section III):

$$z_{\mathrm{SC}}(t) = \frac{1}{\sqrt{2\pi}\,|E_{\mathrm{vac}}|}\int dE_{\alpha_y}\, e^{-\frac{\left(E_{\alpha_y}-E_{\gamma_y}\right)^2}{2|E_{\mathrm{vac}}|^2}}\, z_{E_{\alpha_y},E_{\gamma_x}}(t), \tag{7a}$$

$$I_{\mathrm{vac}} \equiv \frac{1}{2}\epsilon_0 c\,|E_{\mathrm{vac}}|^2 \equiv c\hbar\omega\frac{\sinh^2(r)}{V}, \tag{7b}$$

where $z_{E_{\gamma_x},E_{\alpha_y}}(t)$ is the dipole-moment expectation value induced by a classical driving field $2\epsilon^{(1)}(-\gamma_x \sin(\omega t) + \alpha_y \cos(\omega t))$, and I_{vac} and E_{vac} are the intensity and amplitude of the squeezed vacuum part of the SC state, respectively. The total intensity of the SC beam is given by $I_{\mathrm{tot}} = I_{\mathrm{coh}} + I_{\mathrm{vac}}$, where $I_{\mathrm{coh}} = c\hbar\omega|\gamma|^2/V$ stems from the classical electromagnetic field of the beam and I_{vac} from squeezing.

Equation (7a) allows to calculate the HHG spectrum and the underlying attosecond pulses driven by the squeezed state of light. We evaluate the dipoles $z_{E_{\alpha_y},E_{\gamma_x}}(t)$ by numerically solving equation (4) for a model Ne atom[46]. The resulting attosecond pulses and HHG spectra are depicted in Fig. 1 (all the presented cases exhibit $I_{\mathrm{coh}} = 2\times10^{14}$ W cm^{-2} and $I_{\mathrm{vac}} = 5\times10^{11}$ W cm^{-2}). We find that a phase-squeezed driver creates horn-shaped attosecond pulses and smeared HHG spectra that exhibit a less pronounced exponential cutoff due to increased amplitude uncertainty. In contrast, an amplitude-squeezed driver creates pulse-to-pulse envelope fluctuations in the attosecond pulses and non-integer spectral peaks in the HHG spectra due to increased phase uncertainty. We note that although in the most general case, the emission is given by the photon-number expectation value, the emission shown in Fig. 1 is directly calculated from the single-atom dipole moment. This duality between the photon-number expectation value

https://doi.org/10.1038/s41566-023-01209-w

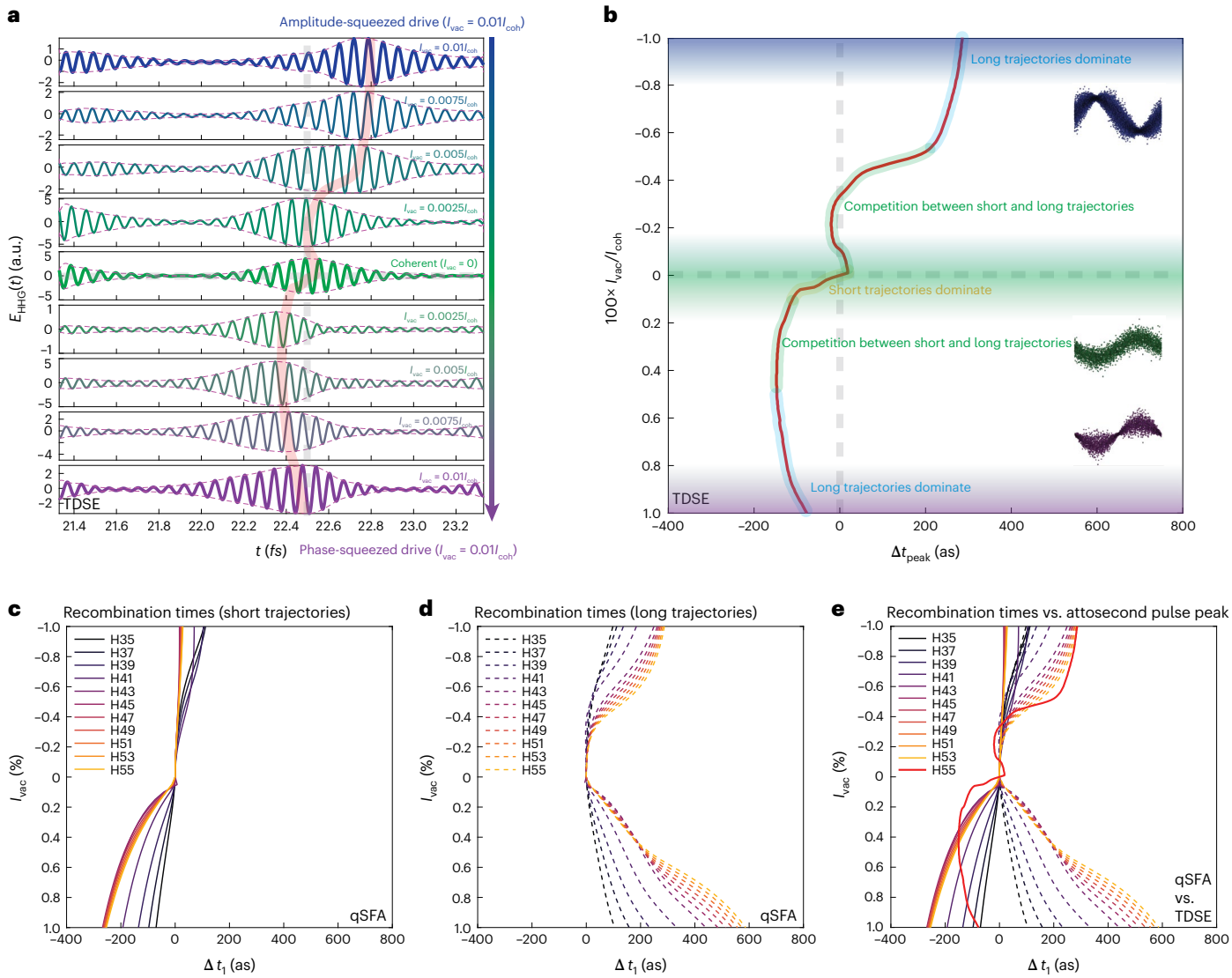

Fig. 3 | Dependence of attosecond pulses on squeezing of the driving field. **a**, TDSE simulations based on equation (7a) provide the attosecond pulse shape for different levels of squeezing. **b**, Peak time of the attosecond pulse t_{peak} as a function of squeezing strength I_{vac} (negative I_{vac} represents amplitude squeezing and positive represents phase squeezing). **c**, Short trajectory recombination times as a function of squeezing for harmonics 35–55. **d**, Long trajectory recombination times for harmonics 35–55. **e**, Both t_{peak} and recombination times displayed on the same graph, showing competition between short and long trajectories as the origin of the complicated squeezing dependence of $t_{peak} = t_{peak}(I_{vac})$.

and single-atom dipole moment is valid in the case of uncorrelated gas[47], but may break down in strongly correlated systems (for example, in a superradiant system[48]).

Electron trajectories in quantized fields

The previous section shows that indeed, in HHG, the emitted attosecond pulses and spectrum are sensitive to the photon statistics of the driving field, and this is reflected in the sensitivity of the underlying material dynamics through the dipole-moment expectation value. Therefore, one also expects the underlying electronic trajectories to be sensitive to photon statistics, even without changing the mean instantaneous electric field of the driver. To quantify the sensitivity of the electronic trajectories to photon statistics, we now employ the saddle point approximation, and derive coupled algebraic equations whose solutions determine the properties of short and long electronic trajectories in an SC laser field. We solve these equations and show that the electronic trajectories and attosecond pulses are strongly modified by the squeezing of the driver's photonic state.

To solve for the electronic trajectories induced by the quantum field, we plug the semi-classical SFA dipole moments $z_\alpha(t)$ into equation (6) (ref. 13):

$$z_\alpha(t) = \frac{\mathrm{i}}{\hbar}\int d^3\mathbf{p}\int_0^t dt' E_\alpha(t)\, d_z(\mathbf{p} - e\mathbf{A}_\alpha(t'))\, d_z^*(\mathbf{p} - e\mathbf{A}_\alpha(t)) \times \mathrm{e}^{-\frac{\mathrm{i}}{\hbar}S_\alpha(\mathbf{p},t',t)} + \text{c.c.}, \tag{8a}$$

$$S_\alpha(\mathbf{p},t',t) \equiv \int_{t'}^{t} dt'' \left(\frac{[\mathbf{p} - e\mathbf{A}_\alpha(t'')]^2}{2} + I_\mathrm{p}\right). \tag{8b}$$

Here $\mathbf{p} = \mathbf{v} + e\mathbf{A}_\alpha(t)$ (ref. 16) and $d_z(\mathbf{v}) = \langle \mathbf{v}|z|0\rangle$, where $|0\rangle$ is the ground state of the atomic system, $|v\rangle$ is a continuum state of velocity $\mathbf{v}$ and the function $S_\alpha(\mathbf{p}, t, t')$ is the semi-classical action of an electron driven by a coherent state $|\alpha\rangle$. Substituting equation (8a) into equation (6) enables us to extract semi-analytical conclusions about the

https://doi.org/10.1038/s41566-023-01209-w

trajectories. Specifically, we can generalize the Lewenstein approach[13] that relies on the saddle point approximation to extract three physically meaningful (and experimentally observable[49]) stationary parameters, namely, $[\mathbf{p}, t' = t_0, t = t_1]$, defining each electronic trajectory. Each frequency component is associated with two trajectories (two sets of stationary parameters), corresponding to the short and long trajectories. Physically, $\mathbf{p}$ is inferred as the canonical momentum of a trajectory, t_0 is the time of ionization and t_1 is the time of recombination.

Plugging equation (8a) into equation (6), we find that in the quantum optical case, the semi-classical action $S_\alpha(\mathbf{p}, t', t)$ is replaced with a quantum optical action $S_q(\mathbf{p}, t', t, \alpha)$:

$$\underbrace{S_q(\mathbf{p}, t', t, \alpha)}_{\text{quantum optical action}} = \underbrace{S_\alpha(\mathbf{p}, t', t)}_{\text{semi-classical action}} + \underbrace{i\log(P(\alpha))}_{\text{photon statistics}}. \quad (9)$$

Similar to the semi-classical case, the emission of high-order harmonics at frequencies $\Omega = n\omega$ mainly originates from the stationary points of $S_q(\boldsymbol{\kappa}_q) - \hbar\Omega t$ with respect to $\boldsymbol{\kappa}_q = [p, t', t, \alpha]$. In the quantum optical picture, each trajectory is characterized by a fourth stationary parameter, which we infer as the dominant coherent component ($\alpha = \alpha_x + i\alpha_y$) associated with the trajectory (Supplementary Section IV). Figure 2 presents the trajectories for a coherent state ($r = 0$; green), phase-squeezed state ($r > 0$; purple) and amplitude-squeezed state ($r < 0$; blue). The solutions for the stationary parameters are displayed in Fig. 2c. Despite all these states differing only in quantum statistics and having identical coherent electric fields, their electronic trajectories display significant qualitative and quantitative shifts. Although we only analyse short and long trajectories, higher-order trajectories[50] are modulated, too, due to correction to the action. To explore the relevance of these stationary solutions to the complete solution of HHG driven by SC light, we perform a time–frequency analysis (Gabor transform) over the dipole accelerations obtained by equation (6) (Fig. 2b). Each Gabor transform is overlaid with the real parts of the recombination times obtained from the stationary parameters of our qSFA theory, showing good agreement between the plots.

Attosecond pulses and the underlying electronic trajectories

Having established a connection between photon statistics, attosecond pulses and electronic trajectories, we now turn to exploring the dependence of the emitted attosecond pulses on the strength of squeezing. This dependence exhibits a complex structure that we explain in terms of short and long trajectories in the quantized fields, as formulated in the previous section. Using equation (7a), we calculate the attosecond pulses generated by the interaction of a model Ne atom with a squeezed state of light, scanning the range of $-0.01 < \mathrm{sign}(r) I_{vac}/I_{coh} < 0.01$; hereafter, we drop the factor $\mathrm{sign}(r)$ for brevity. Here $r < 0$ represents amplitude squeezing, $r > 0$ indicates phase squeezing and $r = 0$ corresponds to a coherent state.

The resulting attosecond pulses are depicted in Fig. 3a. Here the dashed grey lines mark the position of the peak of the attosecond pulse (t_{peak}) for the case of a coherent pulse. The faded red line follows t_{peak} (I_{vac}) for the explored range and is shown by itself in Fig. 3b. In particular, t_{peak} exhibits a strong and complicated dependence on I_{vac}. This dependence can be understood in terms of a competition between the recombination times of short and long trajectories (Fig. 3c,d). For $|I_{vac}|/|I_{coh}| > 0.5\%$, long trajectories display the most significant shifts in recombination times, and hence, they mostly dominate the dependence of t_{peak} on I_{vac}. For the range $|I_{vac}|/|I_{coh}| < 0.1\%$, short trajectories display greater shifts, and hence, the peak of the attosecond pulse is dominated by their recombination times. Finally, in between these ranges, short and long trajectories display comparable shifts in recombination times, resulting in a complicated curve for t_{peak} (I_{peak}). Figure 3e shows t_{peak} and the recombination times of both short and long trajectories on the same graph, illustrating the resemblance and relation between the different curves.

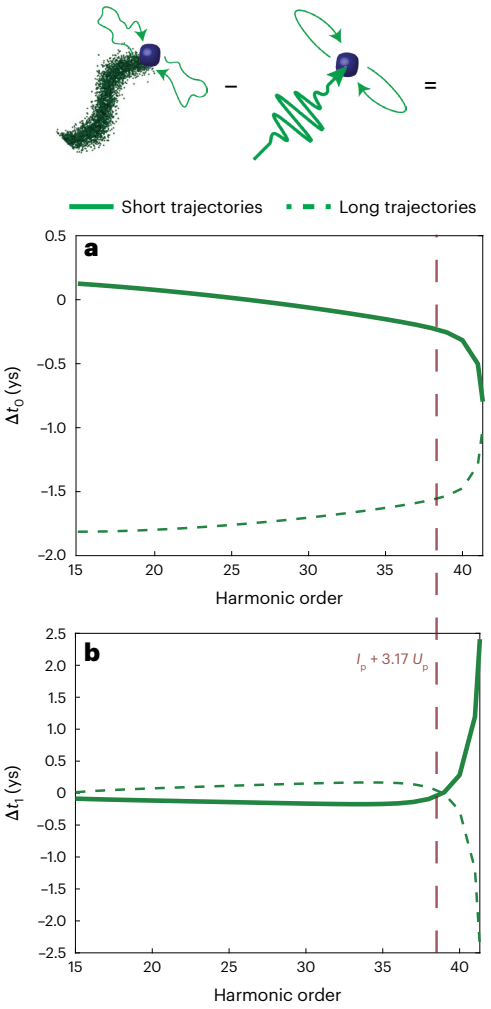

Fig. 4 | Vacuum fluctuations induce yoctosecond time delays in electronic trajectories in HHG. a,**b**, Vacuum-fluctuations-induced corrections to ionization (**a**) and recombination (**b**) times. The calculation is described in detail in Supplementary Section IV.

Discussion

Impact of vacuum fluctuations on HHG

Even seemingly classical driving fields given by an electric field trace $E(t)$ approximate the Glauber coherent state[21], which is a quantum mechanical entity limited by the uncertainty principle and characterized by Poissonian photon statistics (Fig. 4). Interestingly, deviations from classical results are always present because of vacuum fluctuations. Further investigation (Supplementary Section IV) shows that in a typical HHG experiment, the quantum optical correction to the recombination and ionization times is on the order of yoctoseconds (10^{-24} s) (Fig. 4a,b).

Photon-statistics force

The previous sections established a relation between the photon statistics of the driving light and the dynamics of the driven system. This relation naturally hints at the existence of an effective force exerted on the electron by photon statistics, and more specifically, by squeezing. In this section, we show that indeed, for squeezed light, the trajectories obtained from the qSFA theory can be equivalently obtained from an effective semi-classical theory that includes an effective force added to the classical Lorentz force of the driving pulse. We emphasize that although we derive an explicit formula only for squeezed light, an effective photon-statistics force is a general phenomenon in strong-field physics.

https://doi.org/10.1038/s41566-023-01209-w

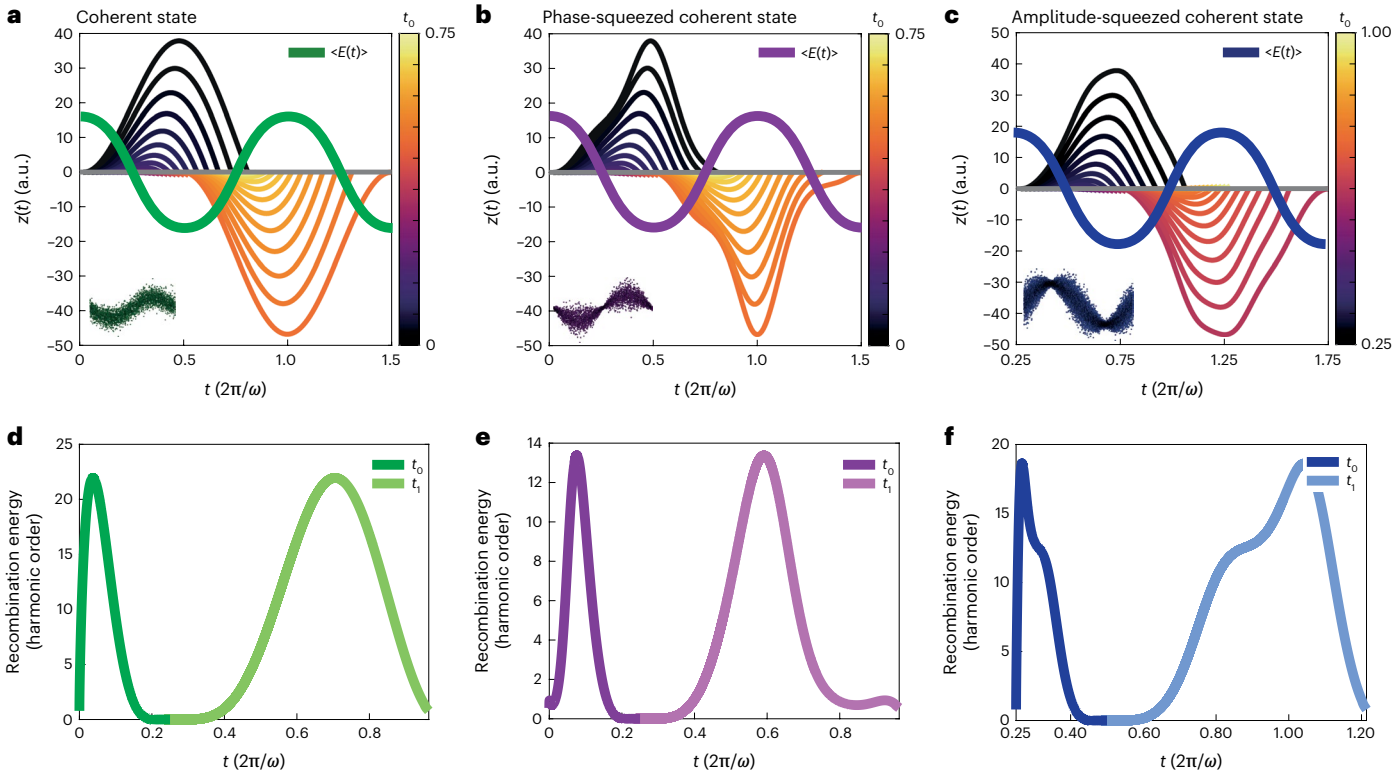

Fig. 5 | Influence of the effective photon-statistics force: Newtonian trajectories. a, Classical Newtonian trajectories driven by a classical electromagnetic wave. **b**,**c**, Newtonian trajectories driven by phase-squeezed (**b**) and amplitude-squeezed (**c**) states of light, corresponding to the effective squeezing force. **d**–**f**, Dispersion of recombination energies for an electron driven by coherent (**d**), phase-squeezed (**e**) and amplitude-squeezed (**f**) states of light.

To derive the photon-statistics force for squeezed light, we begin with the quantum optical action $S_q(\mathbf{p}, t', t, \alpha) = S_\alpha(\mathbf{p}, t', t) + i\log(P(\alpha))$ (equation (9)) with the appropriate $P(\alpha)$ distribution for SC light. We then express the saddle point condition of qSFA: $\nabla_{\boldsymbol{\kappa}_q}\left(S_q\left(\boldsymbol{\kappa}_q\right) - \hbar\Omega t\right) = 0$ as five coupled algebraic equations in the parameters $\boldsymbol{\kappa}_q = [p, t', t, \alpha_x, \alpha_y]$, where $\alpha_{x,y}$ are real-valued quadrature amplitudes. We proceed by solving $\partial_{\alpha_x} S_q = \partial_{\alpha_y} S_q = 0$ and are left with three equations, namely, $\partial_p S_q = \partial_t\left(S_q - \hbar\Omega t\right) = \partial_{t'} S_q = 0$. Finally, we integrate these equations to arrive at an effective semi-classical action $S_{\text{eff}}(\mathbf{p}, t', t)$, which exhibits the same saddle points as the quantum optical action $S_q(\mathbf{p}, t', t, \alpha)$, and is given by

$$S_{\text{eff}}(p, t', t) = \int_{t'}^{t} \mathrm{d}t'' \frac{\left[p - eA_y(t'') - \frac{ie^2}{\omega^2} E_{\text{vac}}^2 \sin(\omega t'') \int_{t'}^{t''} \mathrm{d}\tau v(\tau) \sin(\omega\tau)\right]^2}{2}. \tag{10}$$

Supplementary Sections IV and V provide the detailed derivations. That is, the strong-field dynamics of the electron in the SC field are formally equivalent to the dynamics in an effective semi-classical theory, where the electron is subject to the classical vector potential $A_y(t)$ and an effective photon-statistics force that takes the form of a vector potential $A_{sq}(t)$:

$$A_{sq}(t'') = \frac{ie}{\omega^2} E_{\text{vac}}^2 \sin(\omega t'') \int_{t'}^{t''} \mathrm{d}\tau v(\tau) \sin(\omega\tau). \tag{11}$$

Here E_{vac} is the amplitude of electric-field fluctuations in the anti-squeezed quadrature, which—in our case—is the $\sin(\omega t)$ quadrature of the vector potential. The parameter t' is the initial moment of the dynamics and $v = v(\tau)$ is the velocity at each time. Also, $A_{sq}(t'')$ depends on all the times between t' and t' (current time), that is, it expresses memory in the system.

With such a field in hand, we can derive Newtonian trajectories. Plugging $A_{sq}(t'')$ into equation (8a) for the semi-classical dipole moment, we approximate the motion of the electron in the effective photon-statistics force to be given by

$$z(t'') = e^{-\frac{E_{\text{vac}}^2}{\omega^2} e^2 v(t'') \sin(\omega t'') \int_{t'}^{t''} \mathrm{d}\tau v(\tau) \sin(\omega\tau)} \times z_{SC}(t). \tag{12}$$

Here $z_{SC}(t)$ is constructed out of the saddle point of the original (uncorrected) semi-classical SFA action (the subscript SC stands for semi-classical here). To obtain Newtonian trajectories, we replace $z_{SC}(t)$ with classical trajectories $z_C(t)$ that solve Newton's second law of motion for an electron released at t_0 and driven by $A_y(t)$. The resulting Newtonian trajectories of an electron in coherent, phase-squeezed and amplitude-squeezed states of light are displayed in Fig. 5a–c. The corresponding dispersion of recombination energies for the different cases is plotted in Fig. 5d–f. As shown, the dispersion of recombination energies shows significant dependence on the photon statistics. Phase-squeezed light results in a structurally similar dispersion curve to coherent-state light, but with lower maximal recombination energy. Amplitude-squeezed light results in the maximum recombination energy that is similar to that of a coherent state, but with a significantly modified temporal structure.

Conclusion

We formulated a quantum optical theory of HHG, derived under the SFA. Our theory, termed qSFA, introduces a connection between quantum optics and attosecond science. The qSFA theory directly links

the driving fields' photon statistics, the emitted radiation in the time domain and the underlying electronic trajectories. We have shown that all these features of HHG are modified by the squeezing of the driver photonic state, and we explicitly quantified these effects in an experimentally feasible regime. From a fundamental perspective, our work reveals an effective force that holds the effect of any quantum photon statistics on the electron dynamics. The effect of squeezing on the electronic trajectories also modifies the time delays of the emitted attosecond pulses. This suggests that conventional techniques of attosecond science that resolve electronic trajectories could resolve the effect of quantized fields on electron dynamics. Looking forward, combining our formalism with attosecond science techniques may resolve the role of light–matter entanglement in ultrafast materials dynamics, when it is entangled with light.

Overall, we believe our work will play a central role in the emerging field of extreme-ultraviolet quantum state engineering[32], potentially advancing quantum spectroscopy[51] to the strong-field regime.

Online content

Any methods, additional references, Nature Portfolio reporting summaries, source data, extended data, supplementary information, acknowledgements, peer review information; details of author contributions and competing interests; and statements of data and code availability are available at https://doi.org/10.1038/s41566-023-01209-w.

References

1. Villeneuve, D. M. Attosecond science. *Contemp. Phys.* **59**, 47–61 (2018).
2. Dudovich, N. et al. Measuring and controlling the birth of attosecond XUV pulses. *Nat. Phys.* **2**, 781–786 (2006).
3. Grundmann, S. et al. Zeptosecond birth time delay in molecular photoionization. *Science* **370**, 339–341 (2020).
4. Schultze, M. et al. Attosecond band-gap dynamics in silicon. *Science* **346**, 1348–1352 (2014).
5. Ayuso, D. et al. Synthetic chiral light for efficient control of chiral light–matter interaction. *Nat. Photon.* **13**, 866–871 (2019).
6. Mayer, N., Patchkovskii, S., Morales, F., Ivanov, M. & Smirnova, O. Imprinting chirality on atoms using synthetic chiral light fields. *Phys. Rev. Lett.* **129**, 243201 (2022).
7. Peng, P. et al. Coherent control of ultrafast extreme ultraviolet transient absorption. *Nat. Photon.* **16**, 45–51 (2022).
8. Sainadh, U. S. et al. Attosecond angular streaking and tunnelling time in atomic hydrogen. *Nature* **568**, 75–77 (2019).
9. McPherson, A. et al. Studies of multiphoton production of vacuum-ultraviolet radiation in the rare gases. *J. Opt. Soc. Am. B* **4**, 595–601 (1987).
10. Ferray, M. et al. Multiple-harmonic conversion of 1064 nm radiation in rare gases. *J. Phys. B: At. Mol. Opt. Phys.* **21**, L31–L35 (1988).
11. Krause, J. L., Schafer, K. J. & Kulander, K. C. High-order harmonic generation from atoms and ions in the high intensity regime. *Phys. Rev. Lett.* **68**, 3535–3538 (1992).
12. Corkum, P. B. Plasma perspective on strong field multiphoton ionization. *Phys. Rev. Lett.* **71**, 1994–1997 (1993).
13. Lewenstein, M., Balcou, P., Ivanov, M. Y., L'Huillier, A. & Corkum, P. B. Theory of high-harmonic generation by low-frequency laser fields. *Phys. Rev. A* **49**, 2117–2132 (1994).
14. Luu, T. T. et al. Extreme–ultraviolet high–harmonic generation in liquids. *Nat. Commun.* **9**, 3723 (2018).
15. Ghimire, S. et al. Observation of high-order harmonic generation in a bulk crystal. *Nat. Phys.* **7**, 138–141 (2011).
16. Dromey, B. et al. High harmonic generation in the relativistic limit. *Nat. Phys.* **2**, 456–459 (2006).
17. Paul, P. M. et al. Observation of a train of attosecond pulses from high harmonic generation. *Science* **292**, 1689–1692 (2001).
18. Vampa, G., McDonald, C. R., Orlando, G., Corkum, P. B. & Brabec, T. Semiclassical analysis of high harmonic generation in bulk crystals. *Phys. Rev. B* **91**, 64302 (2015).
19. Li, L. et al. Reciprocal-space-trajectory perspective on high-harmonic generation in solids. *Phys. Rev. Lett.* **122**, 193901 (2019).
20. Amini, K. et al. Symphony on strong field approximation. *Rep. Prog. Phys.* **82**, 116001 (2019).
21. Scully, M. O. & Zubairy, M. S. *Quantum Optics* (Cambridge Univ. Press, 1997).
22. Jechow, A., Seefeldt, M., Kurzke, H., Heuer, A. & Menzel, R. Enhanced two-photon excited fluorescence from imaging agents using true thermal light. *Nat. Photon.* **7**, 973–976 (2013).
23. Manceau, M., Spasibko, K. Y., Leuchs, G., Filip, R. & Chekhova, M. V. Indefinite-mean Pareto photon distribution from amplified quantum noise. *Phys. Rev. Lett.* **123**, 123606 (2019).
24. Spasibko, K. Y. et al. Multiphoton effects enhanced due to ultrafast photon-number fluctuations. *Phys. Rev. Lett.* **119**, 223603 (2017).
25. Qu, Y. & Singh, S. Photon correlation effects in second harmonic generation. *Opt. Commun.* **90**, 111–114 (1992).
26. Iskhakov, T. S., Pérez, A. M., Spasibko, K. Y., Chekhova, M. V. & Leuchs, G. Superbunched bright squeezed vacuum state. *Opt. Lett.* **37**, 1919–1921 (2012).
27. Pérez, A. M. et al. Bright squeezed-vacuum source with 1.1 spatial mode. *Opt. Lett.* **39**, 2403–2406 (2014).
28. Finger, M. A., Iskhakov, T. S., Joly, N. Y., Chekhova, M. V. & Russell, P. S. J. Raman-free, noble-gas-filled photonic-crystal fiber source for ultrafast, very bright twin-beam squeezed vacuum. *Phys. Rev. Lett.* **115**, 143602 (2015).
29. Gao, J., Shen, F. & Eden, J. G. Quantum electrodynamic treatment of harmonic generation in intense optical fields. *Phys. Rev. Lett.* **81**, 1833–1836 (1998).
30. Gao, J., Shen, F. & Eden, J. G. Interpretation of high-order harmonic generation in terms of transitions between quantum Volkov states. *Phys. Rev. A* **61**, 043812 (2000).
31. Tsatrafyllis, N., Kominis, I. K., Gonoskov, I. A. & Tzallas, P. High-order harmonics measured by the photon statistics of the infrared driving-field exiting the atomic medium. *Nat. Commun.* **8**, 15170 (2017).
32. Lewenstein, M. et al. Generation of optical Schrödinger cat states in intense laser–matter interactions. *Nat. Phys.* **17**, 1104–1108 (2021).
33. Lewenstein, M. et al. Attosecond physics and quantum information science. Preprint at https://arxiv.org/abs/2208.14769 (2022).
34. Stammer, P. et al. Quantum electrodynamics of intense laser-matter interactions: a tool for quantum state engineering. *PRX Quantum* **4**, 010201 (2023).
35. Rivera-Dean, J. et al. New schemes for creating large optical Schrödinger cat states using strong laser fields. *J. Comput. Electron.* **20**, 2111–2123 (2021).
36. Stammer, P. et al. High photon number entangled states and coherent state superposition from the extreme ultraviolet to the far infrared. *Phys. Rev. Lett.* **128**, 123603 (2022).
37. Gorlach, A. et al. High harmonic generation driven by quantum light: general formalism and extended cutoff. In *Conference on Lasers and Electro-Optics* FM3B.1 (Optica Publishing Group, 2022).
38. Tsur, M. E. et al. High harmonic generation driven by quantum light: strong-field approximation & attosecond pulses. In *Conference on Lasers and Electro-Optics* FW4B.1 (Optica Publishing Group, 2022).
39. Kim, M. S., de Oliveira, F. A. M. & Knight, P. L. Properties of squeezed number states and squeezed thermal states. *Phys. Rev. A* **40**, 2494–2503 (1989).

40. Grynberg, G., Aspect, A., Fabre, C. & Cohen-Tannoudji, C. *Introduction to Quantum Optics: From the Semi-Classical Approach to Quantized Light* (Cambridge Univ. Press, 2010).
41. Janszky, J. & Yushin, Y. Many-photon processes with the participation of squeezed light. *Phys. Rev. A* **36**, 1288 (1987).
42. Lecompte, C., Mainfray, G., Manus, C. & Sanchez, F. Laser temporal-coherence effects on multiphoton ionization processes. *Phys. Rev. A* **11**, 1009 (1975).
43. Lamprou, T., Liontos, I., Papadakis, N. C. & Tzallas, P. A perspective on high photon flux nonclassical light and applications in nonlinear optics. *High Power Laser Sci. Eng.* **8**, e42 (2020).
44. Heimerl, J. et al. Statistics of multiphoton photoemission under coherent and non-classical illumination. In *Conference on Lasers and Electro-Optics*, Technical Digest Series FM5D.6 (Optica Publishing Group, 2022).
45. Paris, M. G. A. Displacement operator by beam splitter. *Phys. Lett. A* **217**, 78–80 (1996).
46. Tzur, M. E., Neufeld, O., Bordo, E., Fleischer, A. & Cohen, O. Selection rules in symmetry-broken systems by symmetries in synthetic dimensions. *Nat. Commun.* **13**, 1312 (2022).
47. Gorlach, A., Neufeld, O., Rivera, N., Cohen, O. & Kaminer, I. The quantum-optical nature of high harmonic generation. *Nat. Commun.* **11**, 4598 (2020).
48. Pizzi, A., Gorlach, A., Rivera, N., Nunnenkamp, A. & Kaminer, I. Light emission from strongly driven many-body systems. *Nat. Phys.* **19**, 551–561 (2023).
49. Pedatzur, O. et al. Attosecond tunnelling interferometry. *Nat. Phys.* **11**, 815–819 (2015).
50. Milošević, D. B. & Becker, W. Role of long quantum orbits in high-order harmonic generation. *Phys. Rev. A* **66**, 063417 (2002).
51. Kira, M., Koch, S. W., Smith, R. P., Hunter, A. E. & Cundiff, S. T. Quantum spectroscopy with Schrödinger-cat states. *Nat. Phys.* **7**, 799–804 (2011).
52. Lee, R.-K. Squeezed light illustration by QuantumStateDistributions.jl. *GitHub* https://github.com/foldfelis-QO/QuantumStateDistributions.jl (2022).

Data availability
The data supporting the findings of this study are available from the corresponding authors upon reasonable request.

Code availability
The code supporting the findings of this study is available from the corresponding authors upon reasonable request.

Acknowledgements
We thank the Helen Diller Quantum Center for their support. This work was supported by the European Research Council (ERC) under the European Union's Horizon 2020 research and innovation programme (819440-TIMP), and by the Israel Science Foundation (grant no. 1781/18). M.E.T. gratefully acknowledges support from the Council for Higher Education scholarship for excellence in quantum science and technology and the Helen Diller scholarship for excellence in quantum science and technology.

Author contributions
M.E.T. and O.C. initiated this research. A.G. derived the theory presented in Supplementary Section I. M.E.T., M.B. and A.G. derived the theory in Supplementary Section II. M.E.T. and M.B. derived the theory in Supplementary Sections IIIB and IVA. M.E.T. derived the remaining theory, performed the numerical calculations and wrote the first draft of the paper. The project was supervised by O.C., I.K. and M.K. All authors discussed the results and contributed to the writing of the manuscript.

Competing interests
The authors declare no competing interests.

Additional information
Supplementary information The online version contains supplementary material available at https://doi.org/10.1038/s41566-023-01209-w.

Correspondence and requests for materials should be addressed to Matan Even Tzur or Oren Cohen.

Peer review information *Nature Photonics* thanks Maciej Lewenstein, Dejan B. Milosevic and the other, anonymous, reviewer(s) for their contribution to the peer review of this work.